Imaging Agents

DOI: 10.1002/ange.201107026

Deep-Tissue Photoacoustic Tomography of a Genetically Encoded Near-Infrared Fluorescent Probe**

Grigory S. Filonov, Arie Krumholz, Jun Xia, Junjie Yao, Lihong V. Wang, and Vladislav V. Verkhusha**

Non-invasive studies of physiological and pathogenic processes in deep tissues require both new imaging techniques and advanced probes. One of the emerging approaches is photoacoustic (PA) tomography, which is a hybrid technique built on the PA effect.[1] PA imaging relies on the thermoelastic expansion of light-absorbing objects and subsequent production of ultrasonic waves, which are then detected and quantified. PA techniques are highly scalable and can provide high-resolution images in both the transverse and depth directions.[2,3] This combination of the spatial resolution and depth are not achievable by purely optical methods, mostly because of the high degree of light scattering in the tissue.[4] PA imaging has already proved useful for studying vasculature development, blood oxygenation levels, and other processes. Most exploited absorbers are of endogenous origin, such as hemoglobin and melanin, while other contrast agents that are commonly used, such as organic dyes and nanoparticles, need to be delivered into the body from the outside.[5]

Genetically encoded fluorescent proteins (FPs) have revolutionized optical imaging through their exceptional convenience because they can be produced by living cells and tissues, thus eliminating the need for exogenous delivery of contrast reagents.[6] Since FPs are typically strong light absorbers, they should also bring the same convenience and possibilities to the PA approaches. Indeed, the use of conventional FPs of the green fluorescent protein (GFP) family, such as enhanced GFP (EGFP), DsRed, and mCherry, has been demonstrated by photoacoustic imaging of small transparent organisms, such as fruit fly pupa and adult zebrafish.[7] However, the application of conventional GFP-like FPs for PA imaging of mammals is hindered by high hemoglobin absorption below $\lambda = 650$ nm in blood and tissues.

A recently developed bacteriophytochrome-based near-infrared FP, named iRFP,[8] can serve as a probe for PA imaging for several reasons. First, it has a very high intrinsic extinction coefficient of $105\,000\,M^{-1}cm^{-1}$. Second, iRFP's fluorescence quantum yield (QY) is approximately 6%, which ensures a high nonradiative QY that is beneficial for PA imaging. These properties are summarized in Table 1 of the Supporting Information. Third, its absorption and emission spectra lie inside of the near-infrared window for biological tissues, which spans from $\lambda = 650$ to 900 nm. Finally, fluorescence emission of iRFP provides additional options for signal analysis and quantification.

To date, several far-red-shifted GFP-like FPs have been reported, therefore we decided to start by comparing the PA signals from iRFP and the GFP-like proteins. Initial assessment of the theoretical PA properties of iRFP and the most-red-shifted GFP-like proteins, such as E2-Crimson,[9] mNeptune,[10] mKate2,[11] eqFP670,[12] and TagRFP657,[13] clearly indicated the superiority of iRFP (see Table 1 in the Supporting Information). Note that this theoretical assessment did not take into account the substantially more-red-shifted absorption spectrum of iRFP, which coincides with the absorption minimum of oxyhemoglobin (Figure 1a).

To demonstrate that iRFP provides stronger photoacoustic signals than blood at these wavelengths, the following in vitro experiment was performed. The purified iRFP, E2-Crimson, mNeptune, mKate2, eqFP670, and TagRFP657 proteins, together with lysed oxygenated blood (control), were imaged in a PA computed tomography (PACT) setup.[14] The samples were embedded in a gelatin block and imaged using two laser wavelengths ($\lambda = 600$ and 680 nm), which approximately corresponded to the absorption maxima of the proteins. The resulting amplitude of the PACT signal was normalized to the amplitude of the signal for blood (Figure 1b). This method clearly shows the contrast of the PACT signals of the proteins over the intrinsic signal of blood. The contrasts for FPs at $\lambda = 680$ nm were higher than those at $\lambda = 600$ nm, with the 2.2-fold increase of iRFP being the highest. These results justified the choice of bacteriophytochrome iRFP over the far-red GFP-like proteins for PA imaging.

To assess the maximal imaging depth of the iRFP probe, a deep-photoacoustic microscopy (deep-PAM) setup capable of depth-resolved cross-sections was employed.[3] Both iRFP

[*] Dr. G. S. Filonov,[+] Dr. V. V. Verkhusha
Department of Anatomy and Structural Biology, and Gruss-Lipper Biophotonics Center, Albert Einstein College of Medicine
1300 Morris Park Avenue, Bronx, NY 10461 (USA)
E-mail: vladislav.verkhusha@einstein.yu.edu
A. Krumholz,[+] Dr. J. Xia, J. Yao, Dr. L. V. Wang
Department of Biomedical Engineering, Optical Imaging Laboratory
Washington University in St. Louis
One Brookings Drive, St. Louis, MO 63130 (USA)
E-mail: lhwang@seas.wustl.edu
[+] These authors contributed equally to this work.

[**] We thank Bojana Gligorijevic for help with the mice, and Jeffrey Segall for providing the EGFP-expressing MTLn3 cells. We are grateful to Benjamin Glick (University of Chicago), Dmitry Chudakov and Konstantin Lukyanov (both from the Institute of Bioorganic Chemistry, Russia) for the plasmids encoding GFP-like proteins. We thank Yu Zhang and Yunan Xia for help with maintaining cell cultures. We thank James Ballard for help with editing the manuscript. This work was supported by the National Institutes of Health grants GM073913 and CA164468 (to V.V.V.), and in part by EB000712, EB008085, CA134539, and CA136398 (to L.V.W.).

Supporting information for this article is available on the WWW under http://dx.doi.org/10.1002/anie.201107026.

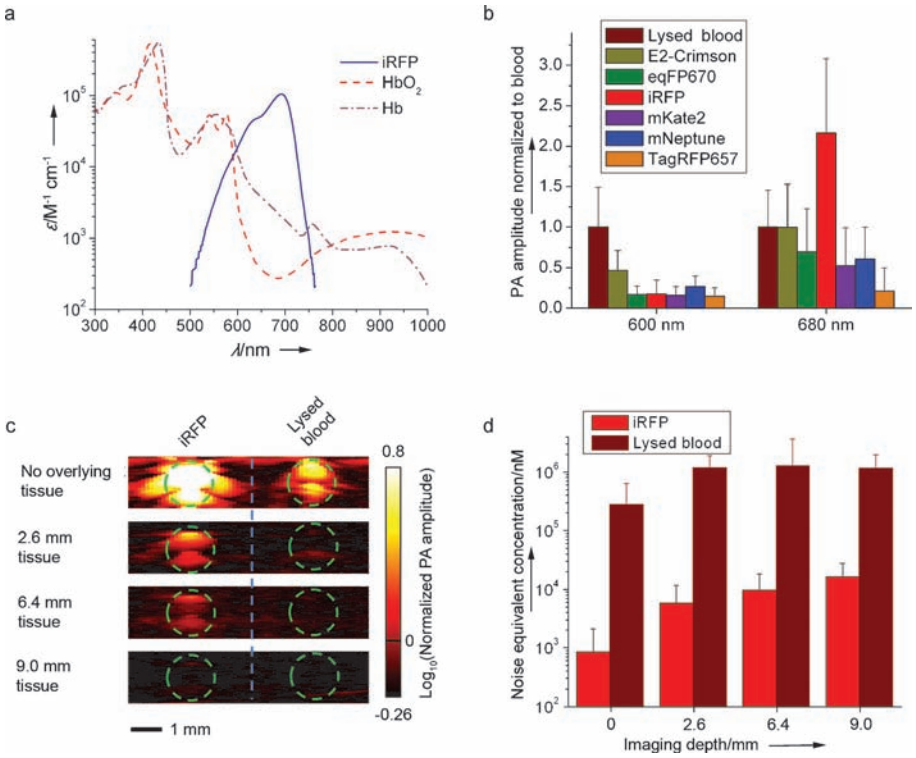

Figure 1. a) Overlay of the molar extinction spectra of oxygenated hemoglobin (HbO_2), deoxygenated hemoglobin (Hb), and iRFP. b) Comparison of PA signal amplitudes of purified iRFP and purified E2-Crimson, eqFP670, mKate2, mNeptune, and TagRFP657 in model gelatin set up at $\lambda = 600$ and 680 nm. PA signal amplitudes were normalized to the amplitude of the signal for blood at the corresponding wavelength. c) Deep-PAM cross-sections of the tubes containing purified iRFP or oxygenated blood with the tissue overlay. Green dashed line indicates the tube boundary. d) Noise equivalent concentration of the deep-PAM technique in nM of the protein (or blood) versus depth.

and lysed oxygenated blood in tubes were imaged with tissue overlays imitating different depths (Figure 1c). Calculations of a noise equivalent concentration (Figure 1d) demonstrated that in the setup used, the iRFP sample with a concentration of approximately 16 μM can be detected up to 9 mm deep in the tissue.

These in vitro results suggested that using $\lambda = 680$ nm excitation light, iRFP should also provide substantially stronger PA signal than blood in vivo, owing to its high extinction coefficient and more-red-shifted spectra. However, an additional concern was yet to be resolved. The iRFP protein, unlike the GFP-like proteins, requires binding of a biliverdin (BV) cofactor to become fluorescent. BV is the enzymatic product of heme, and is endogenously produced in many mammalian tissues.[15] To date, the iRFP fluorescence has only been demonstrated in vivo in the tissues enriched with BV, such as the liver and spleen.[8] Since the concentration of endogenous BV varies in different organs, additional in vivo data were required to support applicability of the iRFP probe to

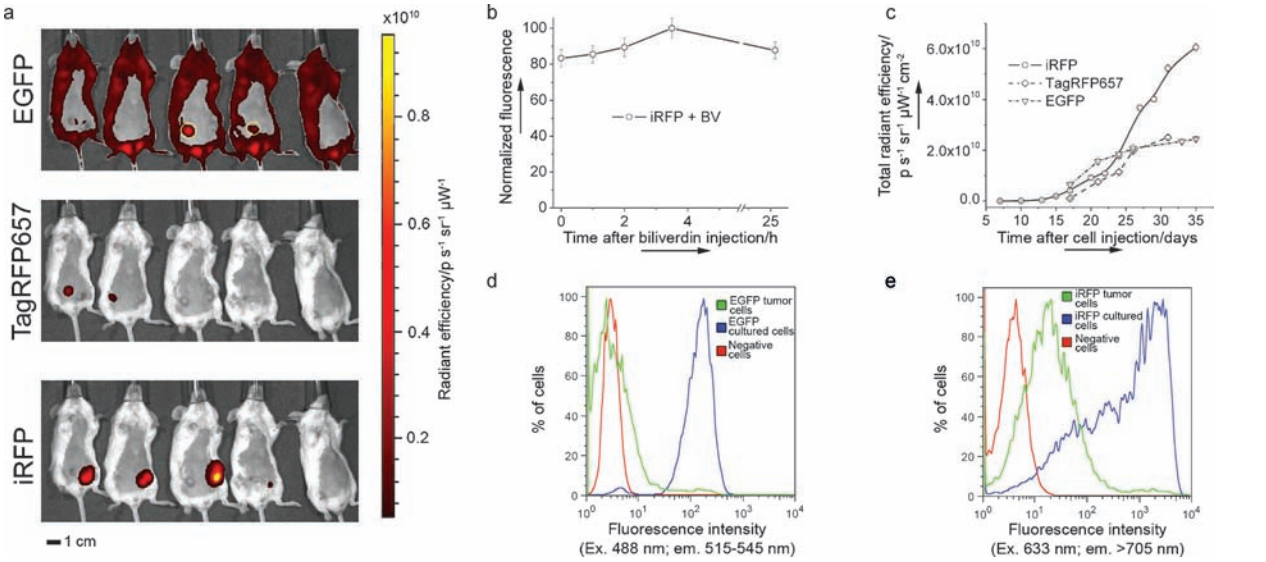

Figure 2. iRFP expression in a mouse tumor xenograft model. a) Bright fluorescence of the iRFP-expressing tumor three weeks after cell injection, in comparison with TagRFP657 and low-contrast EGFP-expressing tumors (circled with yellow). The mouse on the right is the control. The color bar represents radiant efficiency. b) iRFP-expressing tumor brightness change after intravenous BV injection. c) Tumor growth curves plotted based on fluorescence brightness increase of iRFP, TagRFP657, or EGFP. FACS analysis of the cells isolated from the EGFP- (d) or iRFP-expressing (e) tumors five weeks after injection, in comparison with negative MTLn3 cells and the respective preclonal mixture (iRFP) or stable line (EGFP) growing in culture.

other tissues. Conventional fluorescence imaging was chosen to test the applicability.

A preclonal mixture of the rat adenocarcinoma MTLn3 cells stably expressing iRFP was injected into the mammary gland of immunocompromised mice, along with control MTLn3 cells expressing EGFP or far-red TagRFP657. The fluorescent signal at the MTLn3 injection site was first detected in the iRFP channel after just one week (see Figure 1 in the Supporting Information). After three weeks, iRFP expressed in the tumor provided a bright and clear signal with substantially better contrast than the EGFP or TagRFP657 control tumors (Figure 2a). An additional BV injection into the mouse vein only slightly increased the already high iRFP fluorescence intensity (Figure 2b). Injection of the BV directly into the tumor resulted in localized signal enhancement (see Figure 2 in the Supporting Information) which may be helpful in some cases, but not suitable when there is a need to monitor a whole-tumor brightness change over time. Nevertheless, these results demonstrate that injections of exogenous BV is not required to visualize iRFP in tissues other than the liver and spleen.

Monitoring the fluorescence signal allowed us to plot the growth curves for the iRFP-, TagRFP657-, and EGFP-expressing tumors (Figure 2c). EGFP, being the brightest of the protiens used in this experiment on a molecular level, showed only modest in vivo brightness, which is substantially lower than that of iRFP and similar to that of TagRFP657. Moreover, EGFP tumor growth seems to be much slower than in the case of far-red and near-infrared proteins (given that the studied tumors were of a similar size), thus suggesting that blue light, exciting EGFP, does not penetrate as deep into the tumor as it grows, and thus not all EGFP molecules are excited. Again, this demonstrates the superiority of the far-red, and moreover near-infrared FPs for in vivo imaging. Also, simultaneous expression of iRFP and TagRFP657 protiens in one mouse succesfully demonstrated the possibility of the dual color far-red/near-infrared in vivo fluorescent imaging using FPs.

Postmortem fluorescence-activated cell sorting (FACS) analysis of a distribution of the fluorescent cells in the excised tumors additionally confirmed the previously demonstrated noncytotoxicity of iRFP.[8] Indeed, both the EGFP and iRFP tumor cells showed similar ratios between negative and fluorescent cells (ca. 3.5% positive cells; Figure 2d,e). Since EGFP is considered one of the most noncytotoxic standards,[16] these results confirmed that iRFP does not exhibit cytotoxicity.[8]

All these data motivated an in vivo photoacoustic experiment. We exploited the same mouse tumor xenograft model with iRFP-expressing MTLn3 cells, and imaged mice two and three weeks after injecting the cancer cells. Whereas even a two-week-old tumor could be visualized using the PACT and deep-PAM techniques (see Figures 3 and 4 in the Supporting Information), the three-week-old tumor showed a high contrast and imaging depth (Figure 3). During the PACT experiment, images at wavelengths of $\lambda = 700$, 760, and 796 nm were obtained to spectrally resolve iRFP and blood. The position and size of the PACT visualized tumor on the axial mouse cross-section matched those in the photograph (Figures 3a and b). The PACT detection of the iRFP-expressing tumor achieved 100 μm tangential resolution in subcutaneous imaging.

Deep-PAM[3] studies provided both spectral resolution and maximum amplitude projections in three orthogonal planes. Their combination allowed the production of volumetric, spectrally resolved images, with depths up to 4 mm as mimicked by the tissue overlay (Figures 3c and d). In the deep-PAM mode, 280 μm lateral and 75 μm axial resolutions at a depth of 4 mm were achieved, which so far is the best

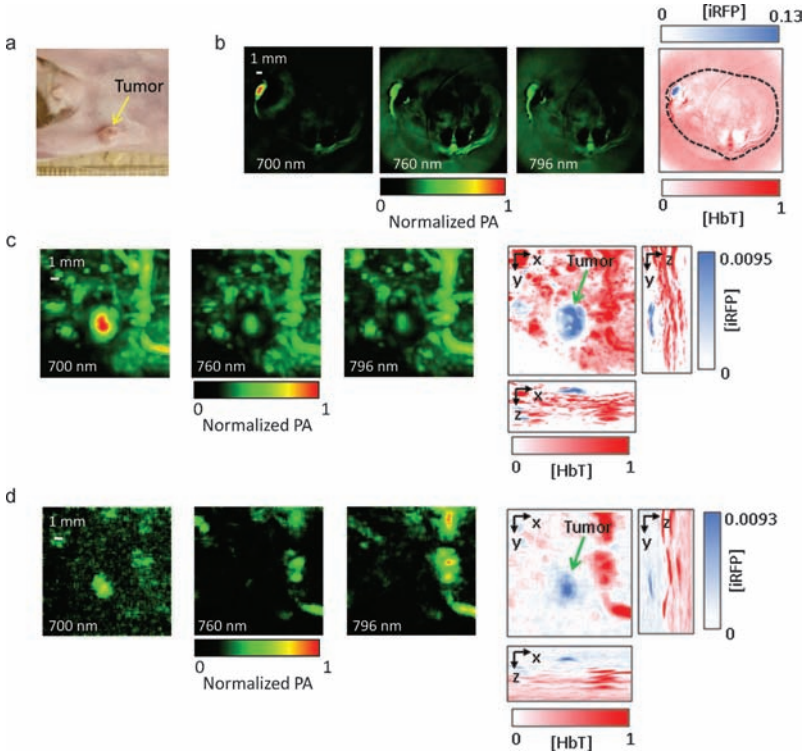

Figure 3. In vivo PACT and deep-PAM imaging of mouse mammary gland tumor. a) Photograph of the mouse with the three-week-old tumor xenograft growing in the mammary pad (yellow arrow). b) PACT image of the tumor shown in the mouse cross-section. The three images on the left were taken at different wavelengths (indicated); the right-most image is a spectrally separated one, with the tumor in blue and the blood in red. The spectrally resolved iRFP signal is normalized to the spectrally resolved signal for blood. The black dashed line shows the mouse body borders. The deep-PAM maximum amplitude projection images of the tumor and surrounding major blood vessels taken without (c) and with (d) 4 mm thick tissue overlay. The three left images on each panel were taken at different wavelengths (indicated), and the images on each of the right-most panels are maximum amplitude projection images with orthogonal orientations; the left and bottom images were used to create the spectrally separated images (in the center). Again, the tumor is labeled blue, the blood is labeled red, and the spectrally resolved iRFP signal is normalized to the spectrally resolved blood signal. The tumor position is indicated by the green arrow.

combination of the depth versus resolution among all currently available genetically encoded probes. Comparing the PA signals of blood and iRFP also provided an estimate of the concentration for the probe of approximately 21 μM.

FPs have brought considerable convenience in monitoring intracellular processes to optical microscopy. However, until recently FPs were only available from the GFP-like family. Excitation and emission of these FPs were limited to the blue, green, and red spectral regions, which made their use in whole-body imaging a challenge.[17] Optical visualization of these FPs inside a mammalian body was feasible only for very large objects, such as terminal cancer tumors,[18] or by employing spectrum-resolving algorithms, such as volumetric tomography[19] or FMT.[20]

Compared to pure optical modalities, PA imaging has substantial advantages, and when combined with proper genetically encoded probes should have greater applicability for whole-body studies in mammals. Owing to its substantially more-red-shifted absorption spectra and high extinction coefficient, the bacteriophytochrome-derived iRFP protein provides significantly higher PA contrast than conventional GFP-like proteins. Similar to the GFP-like proteins, iRFP can be delivered into the body by means of standard genetic manipulations. Moreover, compared to other genetically encoded PA probes, such as beta-galactosidase, iRFP does not require injection of the exogenous substrates.[21] Lastly, the fluorescent properties of the iRFP probe allows using both photoacoustic and fluorescent imaging modalities such as FMT; since this optical approach does not provide microscopic resolution but may have better penetration and thus imaging depth, then it could be a good complement to PA methods. Overall, as demonstrated in this study, the combinations of the iRFP probe with PACT or with deep-PAM techniques can facilitate deep-tissue imaging of the internal tissues and organs by providing high resolution at depths not previously achievable by other genetically encoded probes.

Received: October 5, 2011
Published online: December 23, 2011

Keywords: absorption · cancer · fluorescent proteins · imaging agents · photoacoustic imaging

[1] a) L. V. Wang, *Med. Phys.* **2008**, *35*, 5758 – 5767; b) L. V. Wang, *Nat. Photonics* **2009**, *3*, 503 – 509.
[2] K. Maslov, H. F. Zhang, S. Hu, L. V. Wang, *Opt. Lett.* **2008**, *33*, 929 – 931.
[3] K. H. Song, L. V. Wang, *J. Biomed. Opt.* **2007**, *12*, 060503.
[4] V. Ntziachristos, *Nat. Methods* **2010**, *7*, 603 – 614.
[5] C. Kim, C. Favazza, L. V. Wang, *Chem. Rev.* **2010**, *110*, 2756 – 2782.
[6] a) O. V. Stepanenko, O. V. Stepanenko, D. M. Shcherbakova, I. M. Kuznetsova, K. K. Turoverov, V. V. Verkhusha, *Biotechniques* **2011**, *51*, 313 – 327; b) B. Wu, K. D. Piatkevich, T. Lionnet, R. H. Singer, V. V. Verkhusha, *Curr. Opin. Cell Biol.* **2011**, *23*, 310 – 317.
[7] D. Razansky, M. Distel, C. Vinegoni, R. Ma, N. Perrimon, R. W. Köster, V. Ntziachristos, *Nat. Photonics* **2009**, *3*, 412 – 417.
[8] G. S. Filonov, K. D. Piatkevich, L. M. Ting, J. Zhang, K. Kim, V. V. Verkhusha, *Nat. Biotechnol.* **2011**, *29*, 757 – 761.
[9] R. L. Strack, B. Hein, D. Bhattacharyya, S. W. Hell, R. J. Keenan, B. S. Glick, *Biochemistry* **2009**, *48*, 8279 – 8281.
[10] M. Z. Lin, et al., *Chem. Biol.* **2009**, *16*, 1169 – 1179.
[11] D. Shcherbo, et al., *Biochem. J.* **2009**, *418*, 567 – 574.
[12] D. Shcherbo, et al., *Nat. Methods* **2010**, *7*, 827 – 829.
[13] K. S. Morozova, K. D. Piatkevich, T. J. Gould, J. Zhang, J. Bewersdorf, V. V. Verkhusha, *Biophys. J.* **2010**, *99*, L13 – L15.
[14] J. Gamelin, A. Maurudis, A. Aguirre, F. Huang, P. Guo, L. V. Wang, Q. Zhu, *Opt. Express* **2009**, *17*, 10489 – 10498.
[15] T. J. Mantle, *Biochem. Soc. Trans.* **2002**, *30*, 630 – 633.
[16] T. R. Brazelton, H. M. Blau, *Stem Cells* **2005**, *23*, 1251 – 1265.
[17] B. W. Rice, C. H. Contag, *Nat. Biotechnol.* **2009**, *27*, 624 – 625.
[18] M. Yang, G. Luiken, E. Baranov, R. M. Hoffman, *Biotechniques* **2005**, *39*, 170; M. Yang, G. Luiken, E. Baranov, R. M. Hoffman, *Biotechniques* **2005**, *39*, 172.
[19] G. Zacharakis, H. Kambara, H. Shih, J. Ripoll, J. Grimm, Y. Saeki, R. Weissleder, V. Ntziachristos, *Proc. Natl. Acad. Sci. USA* **2005**, *102*, 18252 – 18257.
[20] N. C. Deliolanis, T. Wurdinger, L. Pike, B. A. Tannous, X. O. Breakefield, R. Weissleder, V. Ntziachristos, *Biomed. Opt. Express* **2011**, *2*, 887 – 900.
[21] L. Li, R. J. Zemp, G. Lungu, G. Stoica, L. V. Wang, *J. Biomed. Opt.* **2007**, *12*, 020504.

